An Empirical Component-Based Model for High-Strength Bolts at Elevated Temperatures

Jonathan M. Weigand[a,1,*], Rafaela Peixoto[b,3], Luiz Carlos Marcos Vieira Junior[b,4], Joseph A. Main[a,1], Mina Seif[a,2]

[a]*Engineering Laboratory, National Institute of Standards and Technology, Gaithersburg, Maryland, United States*
[b]*Department of Structural Engineering, School of Civil Engineering, Architecture and Urban Design, University of Campinas, São Paulo, Brazil*

Abstract

High-strength structural bolts are used in nearly every steel beam-to-column connection in typical steel building construction practice. Thus, accurately modeling the behavior of high-strength bolts at elevated temperatures is crucial for properly evaluating the connection capacity, and is also important in evaluating the strength and stability of steel buildings subjected to fires. This paper uses a component-based modeling approach to empirically derive the ultimate tensile strength and modulus of elasticity for grade A325 and A490 bolt materials based on data from double-shear testing of high-strength 25 mm (1 in) diameter bolts at elevated temperatures. Using these derived mechanical properties, the component-based model is then shown to accurately account for the temperature-dependent degradation of shear strength and stiffness for bolts of other diameters, while also providing the capability to model load reversal.

Keywords: Bolts, Steel, Shear, Elevated temperatures, Fire, Component-based

[*]Corresponding author. Tel.: +1 (301) 975-3302; fax: +1 (301) 869-6275
Email address: jonathan.weigand@nist.gov (Jonathan M. Weigand)

[1]Research Structural Engineer, Materials and Structural Systems Division, Engineering Laboratory, National Institute of Standards and Technology, Gaithersburg, Maryland

[2]Research Structural Engineer, Fire Research Division, Engineering Laboratory, National Institute of Standards and Technology, Gaithersburg, Maryland

[3]Graduate Research Assistant, Department of Structural Engineering, University of Campinas, São Paulo, Brazil

[4]Associate Professor, Department of Structural Engineering, University of Campinas, São Paulo, Brazil

1. Introduction

Steel buildings subjected to structurally significant fires experience thermal assault comprising elevated temperatures and non-uniform thermal gradients, which may induce both temperature-dependent degradation and large unanticipated loads in the steel building components, including connections. The effects of the fire on steel connections are important because, in addition to resisting gravity loads, connections provide critical lateral bracing to the columns. Consequently, failure of steel connections could lead to column instability potentially resulting in local or widespread collapse. High-strength bolts are used in nearly every beam-to-column connection in typical steel building construction practice. Thus, accurately modeling the behavior of the bolts under elevated temperatures is crucial for properly evaluating the connection capacity, and by extension, important in evaluating the strength and stability of steel buildings subjected to fires.

Fire effects on steel structures can produce failures of connections, including fracture of connection plates, shear or tensile rupture of bolts, and bolt tear-out failure of beam webs or connection plates. Seif et al. (2013, 2016) examined such failure modes for typical steel gravity and moment connections at elevated temperatures, using high-fidelity finite element analyses. These studies showed that the potential for failure of connections in fire may result not only from degradation of material strength under the sustained gravity loads, but also on the additional loads and deformations that can be developed through thermal expansion or contraction. The ductility of steel components plays an important role in the performance of connections at elevated temperatures. Sufficient ductility can potentially accommodate thermal expansion and allow for redistribution of loads after failure of one or more individual connection components.

A key issue in predicting the response of structural systems to fire-induced effects is the proper modeling of connection components at elevated temperatures. Gowda (1978), Luecke et al. (2005), and Hu et al. (2009) have examined the behavior of commonly used structural steels at elevated temperatures. Kodur et al. (2012) studied the influence of elevated temperatures on the thermal and mechanical properties of high-strength bolts by conducting shear and tensile coupon testing of 22 mm (7/8 in) diameter high-strength bolts at eight elevated temperatures between ambient temperature and 800 °C. Yu (2006) studied the influence of elevated temperatures on bolted connections, work which included tests of high-strength bolts under shear loading. Yu (2006) observed that bolts did not experience appreciable degradation in their shear resistance until heated in excess of their tempering temperature. More recently, Fischer et al. (2016) tested single-lapped bolted splice joints at temperatures of 400 °C and 600 °C, and Peixoto et al. (2017) tested a large number of high-strength bolts at elevated temperatures under double-shear loading. The tests by Peixoto et al. (2017) used fixtures fabricated from thick heat-treated high-strength plates to minimize the influence of bearing deformations (i.e., to isolate the bolt-shear deformations) which have been significant in previous studies. These recent results by Peixoto et al. (2017) provide sufficient data needed for the development and formulation of reliable component-based models.

This paper describes the development of a reduced-order component-based modeling approach for the shear behavior of high-strength bolts at elevated temperatures that is capable of capturing temperature-induced degradation in bolt-shear strength and stiffness. Semi-empirical models for both ASTM A325 (ASTM, 2014a) and ASTM A490 (ASTM, 2014b) 25 mm (1 in) diameter bolts are developed, based on the comprehensive dataset from Peixoto et al. (2017). Using the component-based model, degradation in the ultimate tensile strength and modulus of elasticity of the bolt materials is linked to the corresponding degradation in the bolt double-shear strength and initial stiffness of the bolt load-deformation response, respectively. By calculating the elevated-temperature-induced degradation in the mechanical properties of the bolt steels, the results of the 25 mm (1 in) diameter bolts can be generalized to calculate the behavior of bolts with other diameters or lap-configurations.

2. Summary of Experimental Data

The component-based model presented in this paper was formulated based on the results of recent double-shear tests of high-strength bolts at elevated temperatures (Peixoto et al., 2017), which covered two bolt grades, three bolt diameters, and five temperatures. The bolt grades were either ASTM A325, with a specified nominal yield strength of 635 MPa (92 ksi) and specified nominal ultimate tensile strength of 825 MPa (120 ksi), or ASTM A490, with a specified nominal yield strength of 895 MPa (130 ksi) and specified nominal ultimate tensile strength of 1035 MPa (150 ksi). For each bolt grade, three diameters of bolts were tested (19 mm (3/4 in), 22 mm (7/8 in), and 25 mm (1 in)) at five temperatures (20 °C, 200 °C, 400 °C, 500 °C, and 600 °C). At least three nominally identical tests were conducted for each combination of parameters.

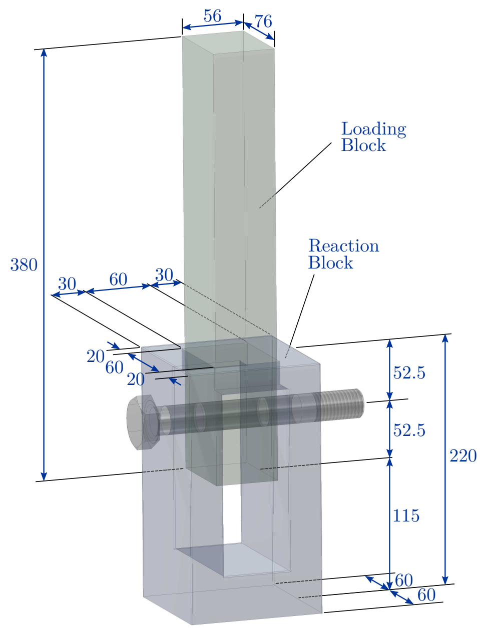

Figure 1: Schematic of bolt double-shear test assembly (dimensions in mm).

The double-shear loads were applied using testing blocks designed to resist loads much larger than the bolts' nominal shear capacity. These blocks were reused for multiple tests. Two sets of testing blocks were manufactured: one set for the 19 mm (3/4 in) and 22 mm (7/8 in) diameter bolts, and one set for the 25 mm (1 in) diameter bolts. The first set was manufactured using ASTM A36 (ASTM, 2014c) steel, with a specified minimum yield strength of 250 MPa (36 ksi), and the second set was manufactured using heat-treated AISI/SAE 8640 alloy steel, with a specified minimum yield strength of 560 MPa (81 ksi). The configuration and dimensions of the testing blocks used to test the 25 mm (1 in) diameter bolts is shown in Fig. 1.

For each test, the entire test setup, including the bolt specimen, was pre-heated to the specified temperature using an electric furnace, and then the loading block (see Fig. 1) was compressed downward with a universal testing machine until the bolt fractured in double-shear. For all tests, both shear planes were located in the unthreaded region of the bolts. The influence of including threads in the shear plane was not considered in this study. Each tested bolt was assigned a unique name, which includes the bolt diameter (specified in mm), bolt grade, temperature level (in °C), and test number. Thus, Test 19A325T20-1 had a diameter of

19 mm (3/4 in), an ASTM A325 grade, and was tested at a temperature of 20 °C (ambient temperature), with the numeral 1 after the hyphen indicating that it was the first test in a set of three nominally identical specimens. Detailed descriptions of the test specimens, test setup, and instrumentation used in the tests are available in Peixoto et al. (2017). Results showed that the shear strength of the bolts was only slightly degraded at a temperature of 200 °C, but the degradation was more significant at higher temperatures. For example, at temperatures of 400 °C, 500 °C, and 600 °C the A325 bolts retained an average of approximately 82 %, 60 %, and 35 % of their initial double-shear strength, respectively. Uncertainties in the measured bolt double-shear load-deformation behavior are reported in Peixoto et al. (2017).

It is noted that in the series of 19 mm (3/4 in) and 22 mm (7/8 in) diameter bolts tested using the ASTM A36 steel testing blocks, large bearing deformations accumulated in the testing blocks, which influenced the measured deformations. However, those bearing deformations were significantly smaller in the AISI/SAE 8640 alloy steel testing blocks used in testing the 25 mm (1 in) diameter bolts, since the ratio of the testing-block strength to the bolt strength was significantly larger. All tested 25 mm (1 in) bolt specimens, whose data were used to formulate the component-based model presented in this paper, used only the AISI/SAE 8640 alloy steel testing blocks.

3. Selection of Data used in Fitting Component-based Model Parameters

The bolt double-shear load-deformation data in Peixoto et al. (2017) had a reduced stiffness at low load levels (e.g., see Fig. 2(a)) due to the initial bearing deformations in the loading and reaction blocks. The stiffness increased as full contact was established between the bolt shaft and the faces of the holes in the testing blocks. The initial-deformation portion of the bolt response is identifiable by the upward concavity of the bolt load-deformation response.

The component-based model for the bolt double-shear load-deformation response was formulated as if the bolt was in full bearing contact with the faces of the holes in the testing blocks at onset of applied loading. Therefore, the parameters for the component-based model were fitted to a subset of the data, corresponding to the data from Peixoto et al. (2017) without the initial reduced-stiffness portions. The portion of the data used in fitting the parameters of the component-based model were selected using the following procedure:

Step 1. Select data from an individual bolt test (Fig. 2(a)).

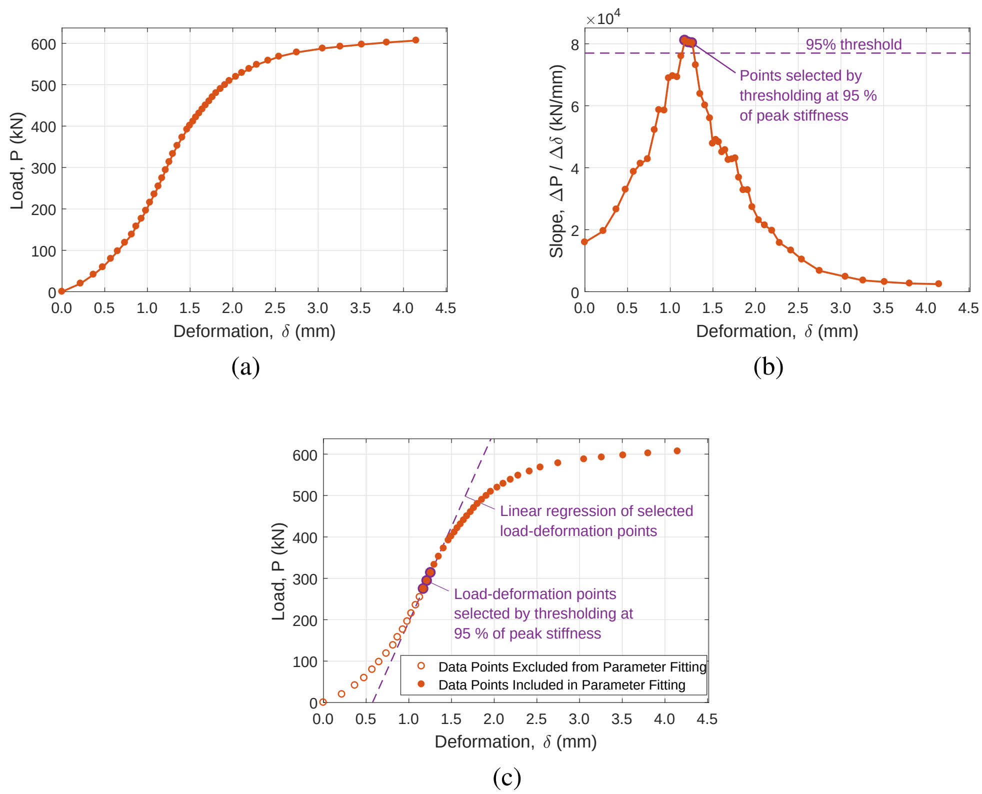

Figure 2: (a) Data from individual bolt load-deformation response, (b) slope of bolt load-deformation response, and (c) selected data to be used in fitting the parameters of the component-based model.

Step 2. Calculate the slope of the bolt load-deformation response (Fig. 2(b)). In this paper, complex step differentiation was used; however, other numerical differentiation methods such as central-differencing are also acceptable.

Step 3. Calculate the initial stiffness as the slope obtained from linear regression of the bolt load-deformation data for which the slope exceeds 95 % of the peak slope. Fig. 2(b) indicates the slope values that exceeded 95 % of the peak slope, and the corresponding load-deformation data points are also indicated in Fig. 2(c).

Step 4. Select data with loads exceeding the regression line to be used in fitting the parameters of the component-based model (Fig. 2(c)).

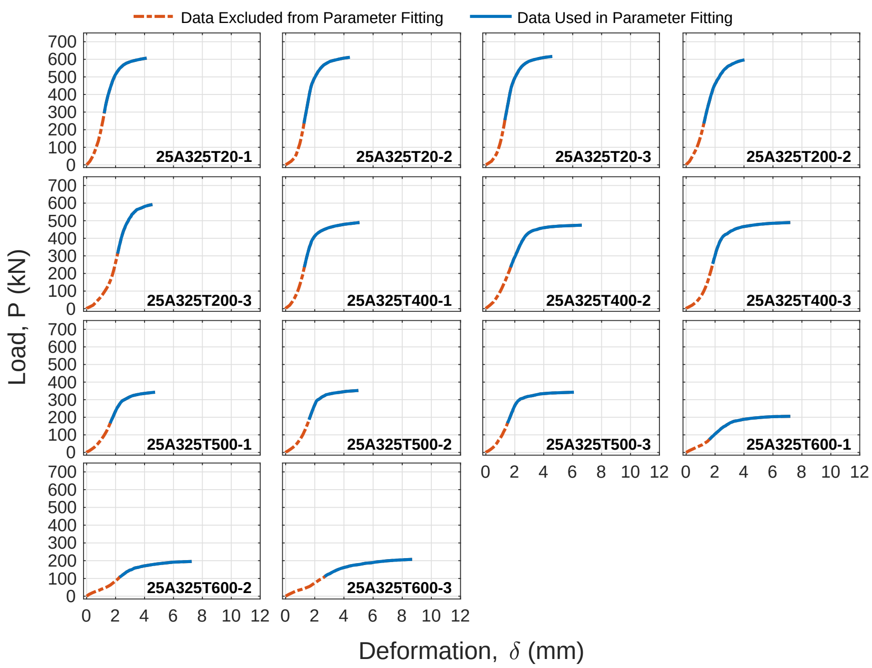

Figure 3: Data used in parameter fitting for 25 mm (1 in) diameter A325 bolt specimens.

Figs. 3 and 4 show the data selected to be used in fitting the parameters of the component-based model for each of the 25 mm (1 in) diameter grade A325 and A490 bolt specimens, respectively. The procedure to exclude data influenced by the initial bearing deformations was applied uniformly across all of the 25 mm (1 in) diameter bolt specimens, and did not influence their double-shear capacity.

4. Component-Based Model

While high-fidelity finite element models permit explicit modeling of the bolt and plate geometries, and provide the capabilities to directly capture complex phenomena such as bearing deformations due to contact between the bolt and plate holes and rupture of the bolt in shear, they may be infeasible for modeling of complete structural systems. Phenomenological component-based models offer considerable advantages in computational efficiency over high-fidelity finite element models, while still providing sufficient resolution to capture the primary characteristics of the response. In component-based models, the individual components of a connection are discretized into component springs, which have fully

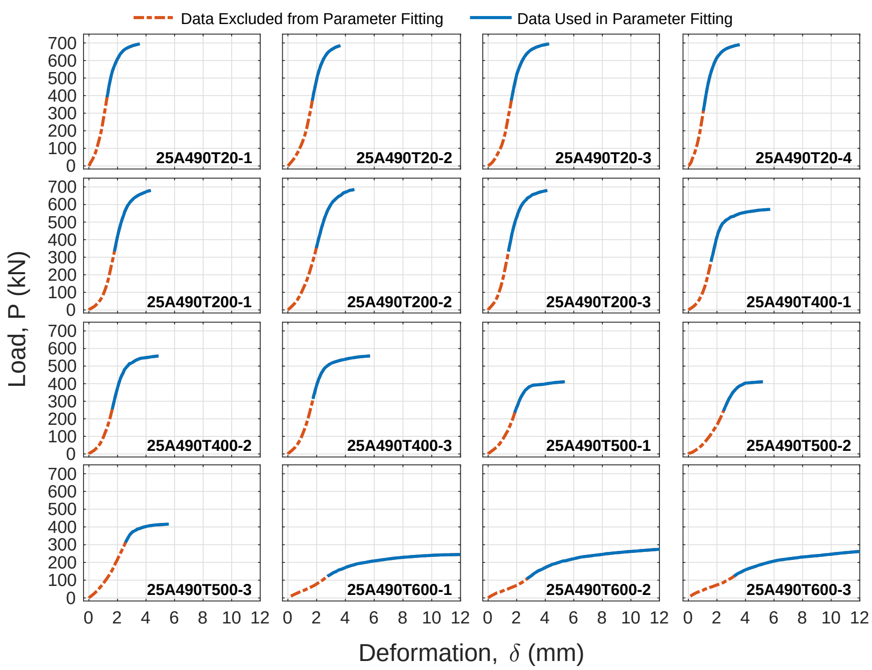

Figure 4: Data used in parameter fitting for 25 mm (1 in) diameter A490 bolt specimens.

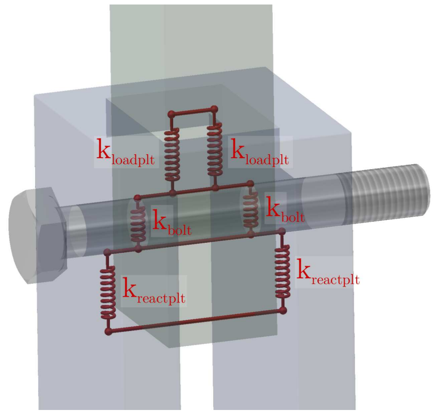

Figure 5: Schematic representation of spring assembly used to model bolt double-shear test assembly.

prescribed strength and stiffness characteristics. In component-based modeling of the double-shear test fixture shown in Fig. 1, each half-length of the bolt would be modeled using three components, representing the bolt shaft (deformable in shear) with initial stiffness k_{bolt}, the loading block with initial stiffness k_{loadplt}, and the reaction block with initial stiffness k_{reactplt} (Fig. 5). However, both direct and indirect measurements showed that deformations in the loading and reaction blocks accounted for less than 1 % of the total deformation in the experimental setup (Peixoto et al., 2017). Thus, for simplicity, bearing deformations in the loading and reaction blocks were ignored (i.e., the loading and reaction blocks were modeled as rigid). The constitutive behavior for the bolts in double-shear was formulated based on a previous component-based model for single-shear behavior in bolts, which was part of a component-based connection model for single-plate shear connections developed by Weigand (2016). The model in Weigand (2016) was previously validated, at ambient temperatures, against double-shear tests of bolts from Weigand (2014) and additionally tests of single-plate shear connections from Crocker and Chambers (2004) and Weigand and Berman (2014).

Isolating the bolt component spring behavior from the model in Weigand (2016), the transverse load-deformation behavior of the bolt, including shear and flexural effects, is modeled using the nonlinear four-parameter "Richard Equation", which was formulated by Richard and Abbott (1975):

$$P(\delta) = \frac{\left(k_{\mathrm{i}} - k_{\mathrm{p}}\right)(\delta - \delta_0)}{\left(1 + \left|\frac{\left(k_{\mathrm{i}}-k_{\mathrm{p}}\right)(\delta-\delta_0)}{r_{\mathrm{n}}}\right|^{n}\right)^{\left(1/n\right)}} + k_{\mathrm{p}}(\delta - \delta_0) \tag{1}$$

where δ is the bolt shear deformation, δ_0 is the initial bearing deformation, k_{i} and k_{p} are elastic and plastic stiffnesses of the bolt double-shear load-deformation response, respectively, n is a shape parameter that controls the sharpness of the transition from the elastic stiffness to the plastic stiffness, and r_{n} is a reference load. Eq. (1) can be extended to include the effects of elevated temperatures on the bolt shear load-deformation response such that

$$P(\delta, T) = \frac{\left(k_{\mathrm{i}}(T) - k_{\mathrm{p}}(T)\right)(\delta - \delta_0(T))}{\left(1 + \left|\frac{\left(k_{\mathrm{i}}(T)-k_{\mathrm{p}}(T)\right)(\delta-\delta_0(T))}{r_{\mathrm{n}}(T)}\right|^{n(T)}\right)^{\left(1/n(T)\right)}} + k_{\mathrm{p}}(T)(\delta - \delta_0(T)) \quad , \tag{2}$$

where (T) denotes dependence of the stiffness or capacity parameter on temperature. Where possible, temperature-dependence is included by incorporating temperature-dependent bolt steel mechanical properties directly into the equations describing the bolt response.

4.1. Calculation of Equation Parameters

While fitted values for the parameters in Eq. (2) were ultimately determined using optimization techniques, first-order approximations for the parameters (typically within 10 % – 40 % of the globally optimized value, depending on the parameter) can be calculated based on linear least-squares regression of the bolt shear load-deformation data, since the Richard Equation has asymptotic limits of k_{i} at $\delta = 0$ and k_{p} at $\delta = \delta_{\mathrm{u}}$ (where δ_{u} is the ultimate deformation of the bolt). These approximate values are used to initialize the optimization scheme, reducing its computational cost and increasing its likelihood of finding the globally optimal solution.

Fig. 6 shows a graphical representation of the calculated first-order approximations for a representative bolt double-shear load-deformation curve. An estimate for the initial stiffness of the bolt double-shear load-deformation response at temperature T, $k_{\mathrm{i}}(T)$, was already previously calculated (in Step 3 of the portion of the data used in fitting the parameters of the component-based model) as the slope of the linear least-squares regression of the bolt load-deformation data exceeding 95 % of the peak slope. The initial bearing deformation is estimated as the value of the initial stiffness regression line at zero load, or

$$\delta_0(T) \approx -\frac{b_{k_\mathrm{i}}(T)}{k_\mathrm{i}(T)} \ , \tag{3}$$

where $b_{k_\mathrm{i}}(T)$ is the constant term of the linear regression. The plastic stiffness $k_\mathrm{p}(T)$ is calculated in a similar manner as the initial stiffness, but as the slope of the linear least-squares regression to the last four points of the bolt load-deformation response at the bolts' maximum plastic deformations. The reference load corresponds to the projection of the plastic stiffness at a deformation of $\delta_0(T)$, and is thus calculated as

$$r_\mathrm{n}(T) \approx b_{k_\mathrm{p}}(T) + k_\mathrm{p}(T)\delta_0(T) \tag{4}$$

where $b_{k_\mathrm{p}}(T)$ is the constant term of the linear least-squares regression defining the plastic stiffness. The initial estimate of the shape parameter was determined using an iterative procedure to minimize the residual between Eq. (2) (using the already-fitted values for temperature-dependent initial stiffness $k_\mathrm{i}(T)$, plastic stiffness $k_\mathrm{p}(T)$, and reference load $r_\mathrm{n}(T)$), and the data from each individual bolt double-shear load-deformation curve.

The globally optimal values for the parameters of Eq. (2) were determined using global optimization (a global search algorithm developed by Ugray et al. (2007) and available in MATLAB's Global Optimization Toolbox (MathWorks, 2016). This algorithm initially executes gradient-based local optimizations from a large number of starting points from within the parameter space, selecting the local optimization result with the minimum objective function value as the starting point to execute the final global optimization. The global search algorithm was initialized using the first-order approximations for the parameters in Eq. (2), which in effect scatters the starting points for the local optimizations in the vicinity of the initial point. Table 1 presents a summary of the final fitted parameters for each individual bolt specimen, and the parameter values are also shown graphically in Figs. 7 and 8 for the 25 mm (1 in) diameter A325 and A490 bolts, respectively.

Replicate tests at each temperature level had relatively consistent double-shear capacities v_n, within 4.5 % of the mean double-shear capacity value for all specimens. Thus, it follows that at each temperature level, the calculated values for the reference load r_n are closely grouped, having the least scatter of the four calculated curve parameters. For both the A325 and A490 bolts, the reference load was only slightly degraded for temperatures up to 200 °C, with more significant

Table 1: Summary of measured and fitted curve parameters for bolt shear data.

Specimen Name	T °C	$k_i(T)$ kN/m (kip/in)	$k_p(T)$ kN/m (kip/in)	$k_p(T)/k_i(T)$ -	$r_n(T)$ kN (kip)	$v_n(T)$ kN (kip)	$n(T)$ -	δ_0 mm (in)
25A325T20-1	20	406246 (2319.7)	9649 (55.1)	0.024	574.1 (129.1)	606.7 (136.4)	4.11	0.46 (0.018)
25A325T20-2	20	563716 (3218.9)	9211 (52.6)	0.016	583.7 (131.2)	612.4 (137.7)	3.11	0.84 (0.033)
25A325T20-3	20	531428 (3034.5)	6938 (39.6)	0.013	594.8 (133.7)	617.0 (138.7)	3.20	0.83 (0.033)
25A325T200-2	200	403817 (2305.9)	12959 (74.0)	0.032	565.7 (127.2)	598.7 (134.6)	3.21	0.64 (0.025)
25A325T200-3	200	447788 (2556.9)	13990 (79.9)	0.031	557.4 (125.3)	594.2 (133.6)	3.48	1.42 (0.056)
25A325T400-1	400	631536 (3606.2)	7541 (43.1)	0.012	461.4 (103.7)	489.7 (110.1)	2.37	0.89 (0.035)
25A325T400-2	400	219143 (1251.3)	3205 (18.3)	0.015	455.6 (102.4)	474.6 (106.7)	5.76	0.63 (0.025)
25A325T400-3	400	581838 (3322.4)	3361 (19.2)	0.006	475.4 (106.9)	491.6 (110.5)	2.11	1.34 (0.053)
25A325T500-1	500	235309 (1343.6)	7358 (42.0)	0.031	315.8 (71.0)	342.6 (77.0)	4.05	0.92 (0.036)
25A325T500-2	500	349763 (1997.2)	5968 (34.1)	0.017	329.8 (74.1)	352.3 (79.2)	3.32	1.07 (0.042)
25A325T500-3	500	317683 (1814.0)	2633 (15.0)	0.008	331.1 (74.4)	343.6 (77.3)	3.02	0.97 (0.038)
25A325T600-1	600	90775 (518.3)	2082 (11.9)	0.023	194.1 (43.6)	206.3 (46.4)	3.58	0.80 (0.032)
25A325T600-2	600	162149 (925.9)	2658 (15.2)	0.016	188.4 (42.3)	197.2 (44.3)	1.73	1.45 (0.057)
25A325T600-3	600	110453 (630.7)	2551 (14.6)	0.023	200.4 (45.1)	208.7 (46.9)	1.72	1.41 (0.055)
Average	-	360832 (2060.4)	6436 (36.8)	0.019	416.3 (93.6)	438.3 (98.5)	3.20	0.98 (0.038)
25A490T20-1	20	475164 (2713.3)	15106 (86.3)	0.032	652.5 (146.7)	696.2 (156.5)	4.54	0.42 (0.016)
25A490T20-2	20	523028 (2986.6)	19773 (112.9)	0.038	643.1 (144.6)	687.9 (154.6)	3.99	0.97 (0.038)
25A490T20-3	20	509413 (2908.8)	11016 (62.9)	0.022	664.2 (149.3)	696.3 (156.5)	3.70	0.87 (0.034)
25A490T20-4	20	552313 (3153.8)	12526 (71.5)	0.023	657.9 (147.9)	691.7 (155.5)	3.72	0.47 (0.019)
25A490T200-1	200	458405 (2617.6)	16297 (93.1)	0.036	632.7 (142.2)	680.1 (152.9)	3.90	1.05 (0.041)
25A490T200-2	200	389630 (2224.8)	20583 (117.5)	0.053	622.3 (139.9)	689.6 (155.0)	4.23	1.06 (0.042)
25A490T200-3	200	467048 (2666.9)	10292 (58.8)	0.022	650.3 (146.2)	680.2 (152.9)	3.84	0.70 (0.027)
25A490T400-1	400	597447 (3411.5)	7078 (40.4)	0.012	544.1 (122.3)	574.2 (129.1)	2.73	1.13 (0.044)
25A490T400-2	400	393286 (2245.7)	7044 (40.2)	0.018	532.4 (119.7)	557.8 (125.4)	4.02	0.98 (0.039)
25A490T400-3	400	456413 (2606.2)	9955 (56.8)	0.022	515.3 (115.8)	560.8 (126.1)	3.57	1.04 (0.041)
25A490T500-1	500	337725 (1928.5)	6022 (34.4)	0.018	386.4 (86.9)	411.0 (92.4)	3.85	1.16 (0.046)
25A490T500-2	500	263709 (1505.8)	4697 (26.8)	0.018	398.6 (89.6)	413.6 (93.0)	4.20	1.52 (0.060)
25A490T500-3	500	323106 (1845.0)	4520 (25.8)	0.014	400.4 (90.0)	417.6 (93.9)	3.55	1.45 (0.057)
25A490T600-1	600	79396 (453.4)	1352 (7.7)	0.017	243.8 (54.8)	247.0 (55.5)	1.85	0.92 (0.036)
25A490T600-2	600	96121 (548.9)	3417 (19.5)	0.036	251.0 (56.4)	280.3 (63.0)	1.72	1.44 (0.057)
25A490T600-3	600	89212 (509.4)	4775 (27.3)	0.054	220.9 (49.7)	279.4 (62.8)	1.79	1.51 (0.060)
Average	-	375714 (2145.4)	9653 (55.1)	0.027	501.0 (112.6)	535.2 (120.3)	3.45	1.04 (0.041)

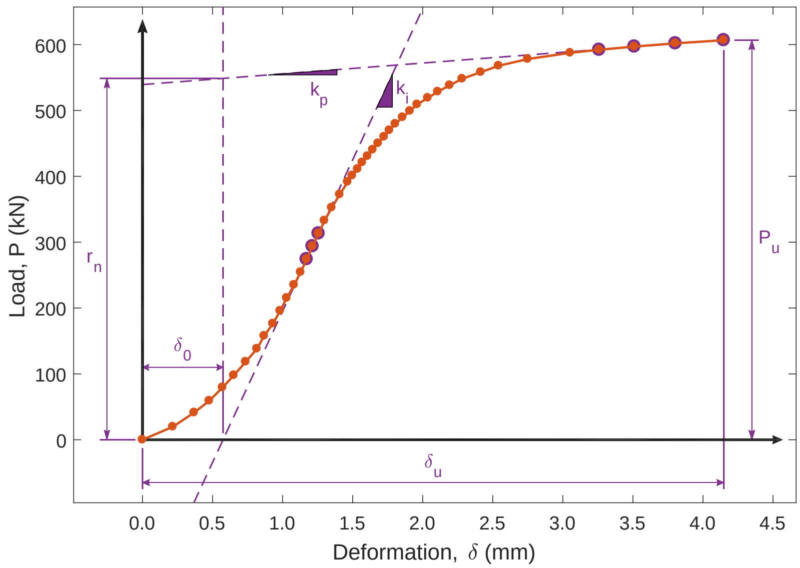

Figure 6: First-order approximation of Richard Equation parameters.

degradation at 400 °C and above. These trends are consistent with observations by Yu (2006), who also found that high-strength bolts did not experience significant degradation in strength at temperatures less than 300 °C.

The other three curve parameters had more scatter in their calculated values for a given temperature. In general, both the initial stiffness and the plastic stiffness of the bolt shear load-deformation curves tended to degrade with increasing temperature. The calculated values for the shape parameter n were usually grouped at a particular temperature; but no systematic trend in their magnitudes with respect to temperature was observed. For both bolt grades, the value of the shape parameter at all temperatures was between 1.5 and 6.0. The scatter in the calculated values of the initial stiffness k_i, plastic stiffness k_p, and shape parameter n at each temperature level did not appear to be adversely influenced by increased temperature, with the scatter in the calculated parameter values at ambient temperature often exceeding that at 600 °C.

Figs. 9(a) and 9(b) show a comparison between Eq. (2) using the parameters fitted via global optimization with data from the 25 mm (1 in) diameter A325 and A490 bolts, respectively, with the initial bearing deformations δ_0 from each test removed for clarity. Fig. 9 shows that use of Eq. (2) with the fitted curve

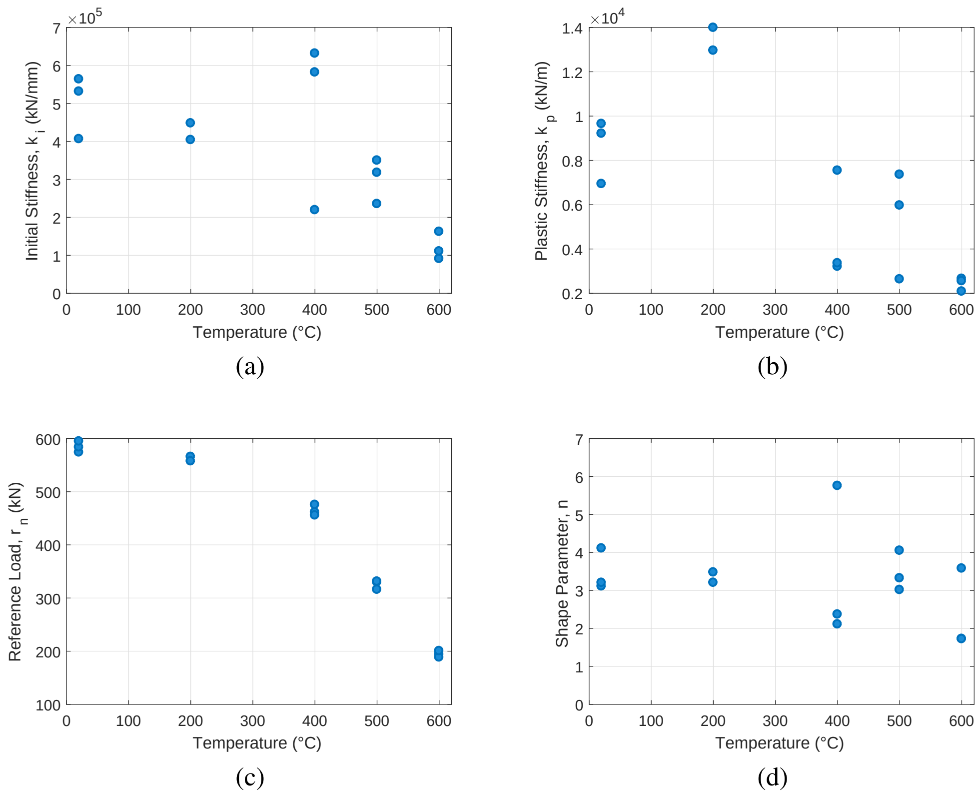

Figure 7: Values of fitted curve parameters for 25 mm (1 in) diameter A325 bolts as a function of temperature: (a) initial stiffness $k_\mathrm{i}(T)$, (b) plastic stiffness $k_\mathrm{p}(T)$, (c) reference load $r_\mathrm{n}(T)$, and (d) shape parameter $n(T)$ (unitless).

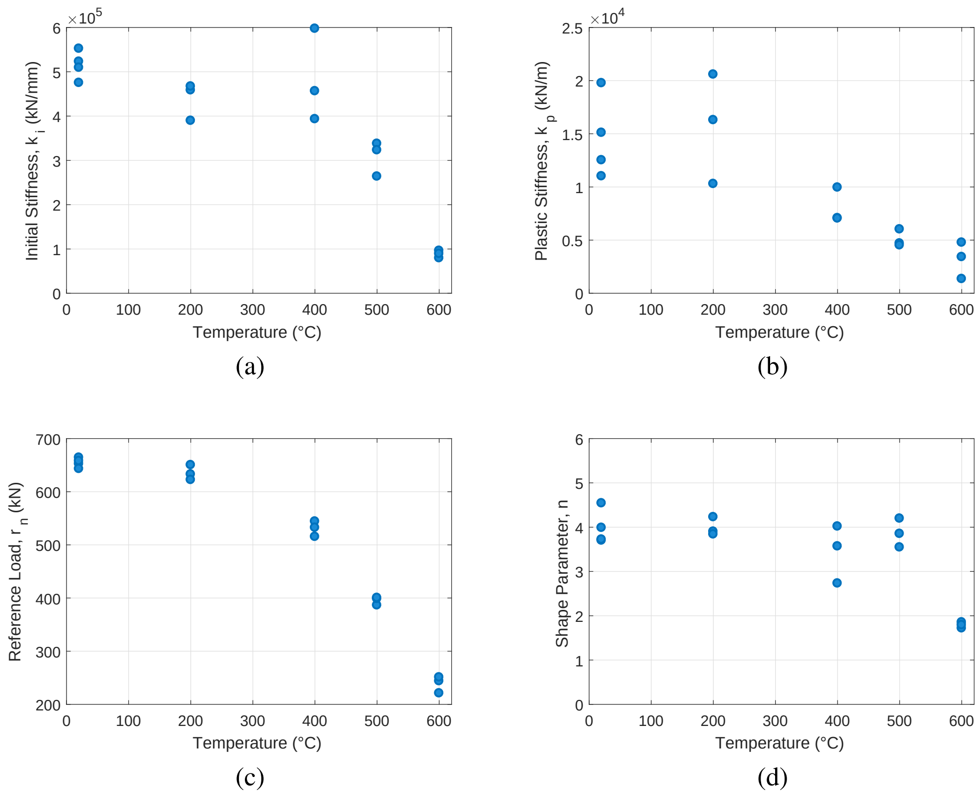

Figure 8: Values of fitted curve parameters for 25 mm (1 in) diameter A490 bolts as a function of temperature: (a) initial stiffness $k_{\mathrm{i}}(T)$, (b) plastic stiffness $k_{\mathrm{p}}(T)$, (c) reference load $r_{\mathrm{n}}(T)$, and (d) shape parameter $n(T)$ (unitless).

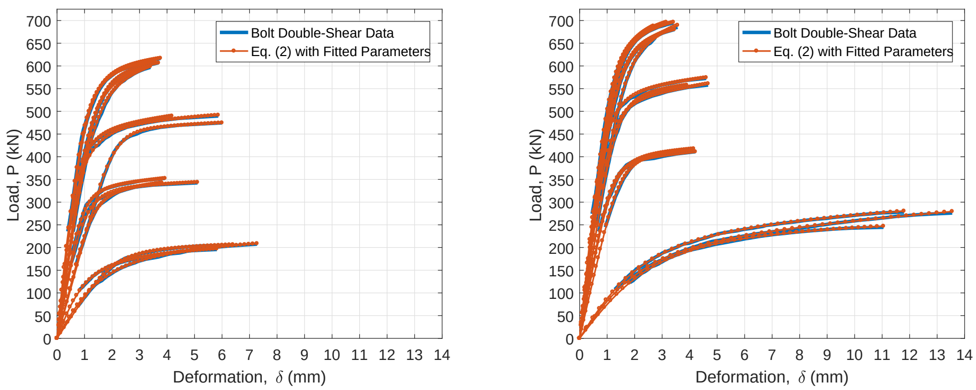

(a) (b)

Figure 9: Comparison between Eq. (1) using fitted curve parameters and experimental data for 25 mm (1 in) diameter (a) A325 bolts and (b) A490 bolts.

parameters provided in Table 1 matches the experimental data within 3 % across all bolt tests.

4.2. Temperature-Dependent Models for Bolt Mechanical Properties

To develop an approach that can predict the shear load-deformation response of the 19 mm (3/4 in) and 22 mm (7/8 in) diameter bolts using the data from the 25 mm (1 in) bolts, the bolt-shear component-based model from Weigand (2016) is used to transform the reference load and initial stiffness data into the ultimate tensile strength and modulus of elasticity, respectively, of the bolt steel. Next, equations are fitted to the data for the ultimate tensile strength and modulus of elasticity, providing temperature-dependent expressions for these mechanical properties, which should be relatively consistent between bolts of different diameters. Piece-wise linear equations are also fitted to the data for the plastic stiffness and shape parameter to facilitate complete double-shear modeling of the bolt response at elevated temperatures.

The ultimate tensile strength of the bolt steels, $F_{\mathrm{u}}(T)$, can be related to the shear capacity via the equation for the temperature-dependent double-shear capacity of the bolt, $v_{\mathrm{n}}(T) = n_{\mathrm{sp}} 0.6 A_{\mathrm{b}} F_{\mathrm{u}}(T)$, where $n_{\mathrm{sp}} = 2$ is the number of shear planes through the bolt, and $A_{\mathrm{b}} = (\pi/4)\, d_{\mathrm{b}}^2$ is the bolt cross-sectional area. The bolt steel ultimate tensile strength can be written in terms of the double-shear capacity

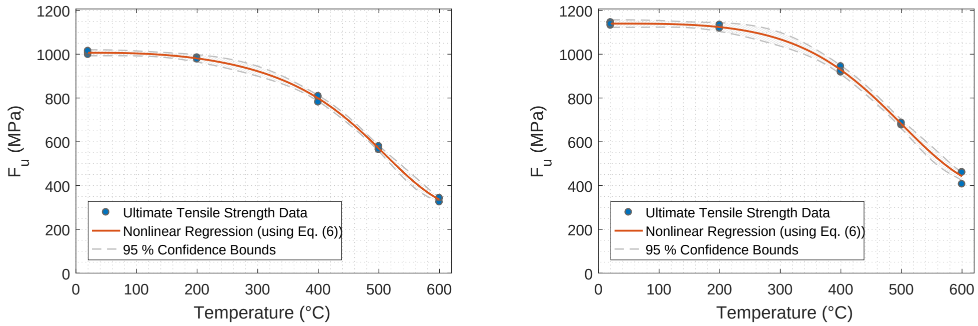

(a) (b)

Figure 10: Ultimate tensile strength, fitted using Eq. (6), for 25 mm (1 in) diameter (a) A325 bolts and (b) A490 bolts. Hatched area corresponds to 95 % confidence interval.

of the bolt such that

$$F_{\mathrm{u}}(T) = \frac{v_{\mathrm{n}}(T)}{n_{\mathrm{sp}} 0.6 A_{\mathrm{b}}} \quad . \tag{5}$$

The discrete markers in Fig. 10 show the values for the ultimate tensile strength calculated using Eq. (5).

To characterize the ultimate tensile strength over the full range of temperatures of interest, an exponential function of the form:

$$F_{\mathrm{u,fitted}}(T) = F_{\mathrm{u,amb}} \left(a_1 + (1 - a_1) \exp\left(-\frac{1}{2} \left(\left(\frac{T - T_{\mathrm{amb}}}{a_2} \right)^{a_3} + \left(\frac{T - T_{\mathrm{amb}}}{a_2} \right)^{a_4} \right) \right) \right) \tag{6}$$

was fitted to the experimental data using nonlinear least-squares regression techniques (Fig. 10). The ambient-temperature ultimate tensile strength $F_{\mathrm{u,amb}}$ was fitted to the data along with the other coefficients. The fitted coefficients of Eq. (6), $F_{\mathrm{u,amb}}$ and a_1 through a_4, are shown in Table 2 along with their 95 % confidence bounds. The 95 % confidence bounds are also shown on Fig. 10 as dashed lines, with the hatched area between the confidence bounds comprising the 95 % confidence interval. The 95 % confidence bounds form a narrow band enclosing the respective fits to the ultimate tensile strength data, indicating that the variance in the measured ultimate tensile strengths is relatively small.

Independent tensile testing of coupons machined from the 25 mm (1 in) diameter A325 and A490 bolts measured the ambient-temperature ultimate tensile strengths for the A325 and A490 bolts at 950.9 MPa (137.9 ksi) and 1126.7 MPa (163.4 ksi), respectively, which are within 6 % and 1 %, of the values of $F_{\mathrm{u,amb}}$

Table 2: Summary of fitted curve parameters for bolt mechanical properties.

	Grade A325		Grade A490		
Fit Type	Coeff. Value	95 % Confidence Bounds (lower, upper)	Coeff. Value	95 % Confidence Bounds (lower, upper)	units
Ultimate Tensile Strength (Eq. (6))	$F_{u,amb}$ = 1007 (146.0)	(993 (144.0), 1020 (148.0))	$F_{u,amb}$ = 1140 (165.3)	(1122 (162.8), 1157 (167.8))	MPa (ksi)
	a_1 = 0.2758	(0.1591, 0.3925)	a_1 = 0.3141	(0.1211, 0.5072)	°C
	a_2 = 488.7	(456.9, 520.5)	a_2 = 492.7	(435.3, 550.2)	°C
	a_3 = 7.291	(3.924, 10.659)	a_3 = 6.251	(0.766, 11.736)	-
	a_4 = 2.649	(1.767, 3.531)	a_4 = 3.207	(1.334, 5.079)	-
Modulus of Elasticity (Eq. (14))	E_{amb} = 170.13 (24675)	(118.92 (17248), 221.34 (32102))	E_{amb} = 175.47 (25450)	(154.39 (22392), 196.56 (28508))	GPa (ksi)
	g_1 = -0.0004083	(-0.0011032, 0.0002867)	g_1 = -0.0004835	(-0.0007801, -0.0001869)	$°C^{-3}$
	g_2 = 0.2631	(-0.3700, 0.8962)	g_2 = 0.3184	(0.0551, 0.5818)	$°C^{-2}$
	g_3 = -48.48	(-197.69, 100.73)	g_3 = -59.25	(-119.67, 1.18)	$°C^{-1}$

fitted to the bolt double-shear data. The close agreement between the fitted values and measured ultimate tensile strengths at ambient temperature provides evidence that Eq. (5) is appropriate, and lends credibility to the approach of using the more numerous (in the current study) double-shear strength data to estimate the ultimate tensile strength of the bolt materials.

The modulus of elasticity of the bolt steels can be related to the initial stiffness of the bolts using Eq. (20) from Weigand (2016), but adjusted for the two shear planes through the bolt in double-shear testing, and incorporating temperature-dependence such that:

$$k_{\mathrm{i}}(T) = \frac{n_{\mathrm{sp}}}{\frac{1}{k_{\mathrm{br}}(T)} + \frac{1}{k_{\mathrm{v}}(T)}} \quad , \tag{7}$$

with bearing stiffness

$$k_{\mathrm{br}}(T) = \frac{1}{1+3\beta_{\mathrm{b}}}\left(\frac{t_{\mathrm{RB}} t_{\mathrm{LB}} E(T)}{2\left(t_{\mathrm{RB}} + t_{\mathrm{LB}}\right)}\right) \quad , \tag{8}$$

and shearing stiffness

$$k_{\mathrm{v}}(T) = \frac{12 E(T) I_{\mathrm{b}}}{L_{\mathrm{b}}^{3}(1+\Phi(T))} \quad . \tag{9}$$

In Eqs. (8) and (9), β_{b} is a correction factor that accounts for the concentration of bearing forces at the interface between plates ($\beta_{\mathrm{b}} = 1$ for shear was used in this study, see Nelson et al. (1983) for more details), $I_{\mathrm{b}} = \left(\pi d_{\mathrm{b}}^{4}\right)/64$ is the moment of inertia of the bolt shaft cross-section, $L_{\mathrm{b}} = (1/2)\left(t_{\mathrm{RB}} + t_{\mathrm{LB}}\right)$ is the bolt length at each shear plane where t_{RB}=30 mm (1.18 in) is the thickness of the reaction block, and where t_{LB}=56 mm (2.20 in) is the thickness of the loading block.

$$\Phi(T) = \frac{12E(T)I_{\mathrm{b}}}{L_{\mathrm{b}}^2}\left(\frac{1}{\kappa G(T)A_{\mathrm{b}}}\right) \tag{10}$$

is a term in Timoshenko beam theory that characterizes the relative importance of the shear deformations to the bending deformations (e.g., see Thomas et al. (1973)), $G(T) = E(T)/\left(2\left(1+\nu\right)\right)$ is the bolt shear modulus, $\nu = 0.29$ (assumed over all temperatures) is Poisson's ratio, and κ is the shear coefficient for a circular cross-section, defined as:

$$\kappa = \frac{1}{\frac{7}{6} + \frac{1}{6}\left(\frac{\nu}{1+\nu}\right)^2} \quad . \tag{11}$$

The modulus of elasticity of the bolt steel is determined by solving Eq. (7) for $E(T)$ such that:

$$E(T) = \gamma k_{\mathrm{i}}(T) \quad , \tag{12}$$

where

$$\gamma = \frac{2(t_{\mathrm{RB}} + t_{\mathrm{LB}})\left(3\left(1+3\beta_{\mathrm{b}}\right)\pi d_{\mathrm{b}}^4\left(1+\nu\right) + d_{\mathrm{b}}^2(7+2\nu(7+4\nu))t_{\mathrm{RB}}t_{\mathrm{LB}} + \left(1+\nu\right)t_{\mathrm{RB}}t_{\mathrm{LB}}\left(t_{\mathrm{RB}}+t_{\mathrm{LB}}\right)^2\right)}{n_{\mathrm{sp}}\left(3\pi d_{\mathrm{b}}^4(1+\nu)t_{\mathrm{RB}}t_{\mathrm{LB}}\right)} \quad . \tag{13}$$

Similar to the approach taken for the ultimate tensile strength, an equation was fitted to the modulus of elasticity data to enable its calculation for all temperatures. For the modulus of elasticity, a third-order polynomial equation of the form:

$$E_{\mathrm{fitted}}(T) = E_{\mathrm{amb}}\left(g_1(T - T_{\mathrm{amb}})^3 + g_2(T - T_{\mathrm{amb}})^2 + g_3(T - T_{\mathrm{amb}}) + 1\right) \tag{14}$$

was fitted to the experimental data using least-squares regression techniques. Coefficients g_1 through g_4 are shown in Table 2. Fitted curves using Eq. (14) are shown in Fig. 11 as solid lines. As a result of the larger variances in the modulus of elasticity data, the 95 % confidence intervals calculated for the fitted modulus of elasticity curves are significantly wider than those calculated for the ultimate tensile strength.

Due to the significant scatter in the data for the plastic stiffness (see Figs. 7(b) and 8(b)), a different approach was used to calculate it. The relationship between the plastic stiffness and the elastic stiffness, at a particular temperature, was determined as the average of the $k_{\mathrm{p}}(T)/k_{\mathrm{i}}(T)$ values from Table 1 (Fig. 12), and the plastic stiffness was calculated as this ratio multiplied by specimen-specific initial stiffness. The shape parameter n, while influencing the bolt double-shear response

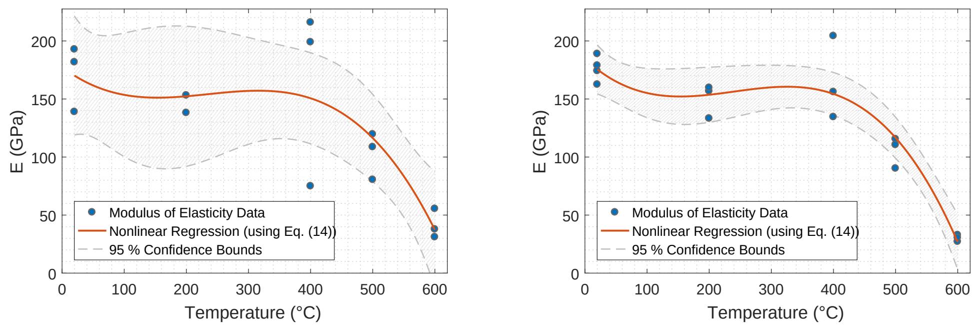

(a) (b)

Figure 11: Modulus of elasticity, fitted using Eq. (14), for 25 mm (1 in) diameter (a) A325 bolts and (b) A490 bolts. Hatched area corresponds to 95 % confidence interval.

at the transition from elastic to plastic deformations, has relatively little influence on the calculated capacity of the bolts. Thus, the value of n was simply chosen as the average value at each individual temperature. The data from Peixoto et al. (2017) showed no systematic influence of bolt diameter of the double-shear deformation at failure, and thus the deformations at failure was similarly chosen as the average value at each temperature. Since the stiffness of the bolt double-shear response had significantly decreased at the ultimate deformations, choosing averaged values for the ultimate deformation capacities had only a minor influence on the calculated bolt reference loads.

Figs. 14(a) and 14(b) show comparisons of the component-based model, with parameters fitted using Eq. (6), Eq. (14), and the approaches for calculating k_{p} and n described above, to the experimental data for the 25 mm (1 in) diameter bolts.

5. Application of Modeling Approach to Smaller-Diameter Bolts

The empirical bolt load-deformation modeling approach is based solely on the data from Peixoto et al. (2017) for the 25 mm (1 in) diameter A325 and A490 bolts. In this section, the capabilities of the modeling approach in predicting temperature-dependent capacities for the bolts are tested against data from the 19 mm (3/4 in) and 22 mm (7/8 in) diameter bolts in Peixoto et al. (2017). It is challenging to directly compare the load-deformation responses for the bolts, due to the effects of excessive bearing deformations in the loading and reaction blocks used for the 19 mm (3/4 in) and 22 mm (7/8 in) diameter bolt tests (as described in Section 2). As an example, Fig. 15 shows the effect of the accumulated bearing

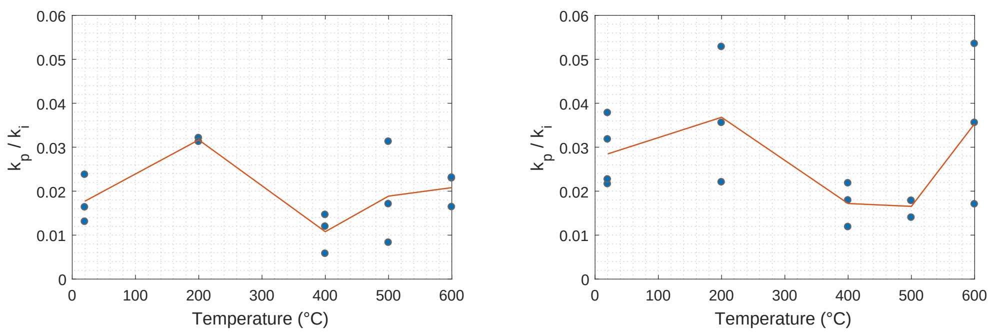

(a) (b)

Figure 12: Fitted ratio of plastic stiffness to initial stiffness for 25 mm (1 in) diameter (a) A325 bolts and (b) A490 bolts.

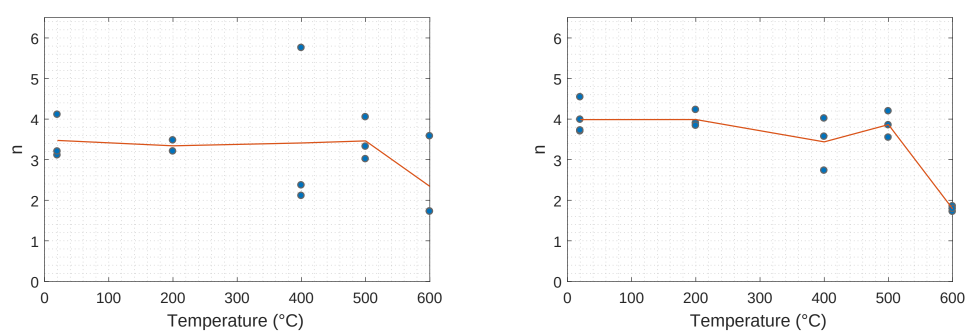

(a) (b)

Figure 13: Fitted shape parameter for 25 mm (1 in) diameter (a) A325 bolts and (b) A490 bolts.

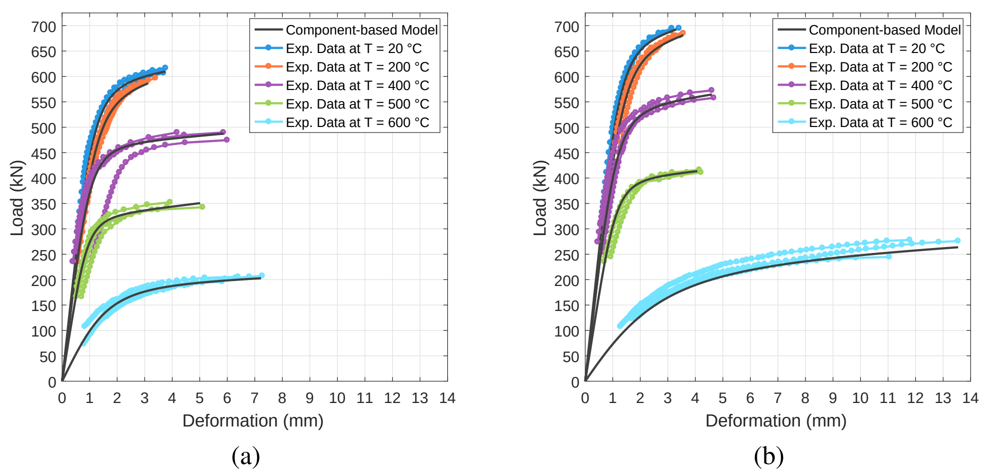

Figure 14: Comparison of component-based model to experimental data for 25 mm (1 in) diameter (a) A325 bolts and (b) A490 bolts.

deformations by comparing results from the first 19 mm (3/4 in) diameter bolt test (19A325T20-1), in which the virgin loading and reaction blocks were used, with results from the third 19 mm (3/4 in) diameter bolt test (19A325T20-3). However, since the accumulated bearing deformations had relatively little influence on the bolt double-shear capacity (as demonstrated by Fig. 15), the double-shear capacities of the 19 mm (3/4 in) and 22 mm (7/8 in) diameter bolts can be objectively compared.

The bolts are modeled using Eq. (2), with (i) initial stiffness determined from Eq. (7), incorporating temperature-dependence via Eq. (14) (Fig. 11) for the modulus of elasticity, (ii) plastic stiffness determined as a function of the initial stiffness, using the ratios shown in Fig. 12, (iii) shape parameter taken as the average value at each temperature (see Fig. 13), and reference load calculated as

$$r_{\mathrm{n}} = n_{\mathrm{sp}} 0.6 A_{\mathrm{b}} F_{\mathrm{u}}(T) \left(\delta_{\mathrm{u}} - \delta_0\right) \tag{15}$$

using the fitted ultimate tensile strength (Eq. (6), Fig. 10). The bolt-shear deformation capacities at failure were assumed to be equivalent to the average deformation capacities of the corrected 25 mm (1 in) diameter bolt data.

Tables 3 and 4 show that the empirically-fitted modeling approach predicts the capacity of the 19 mm (3/4 in) and 22 mm (7/8 in) bolts within an average difference of less than 3.5 %. A negative value for the percent error indicates that

Table 3: Summary of measured and predicted double-shear capacities for 19 mm (3/4 in) and 22 mm (7/8 in) diameter A325 high-strength bolts.

Specimen Name	T °C	Meas. Failure Load, kN (kip)	Pred. Failure Load, kN (kip)	Percent Difference
19A325T20-1	20	372.3 (83.7)	379.9 (85.4)	2.0
19A325T20-2	20	375.4 (84.4)		1.2
19A325T20-3	20	391.9 (88.1)		-3.1
19A325T200-1	200	384.3 (86.4)	370.2 (83.2)	-3.7
19A325T200-2	200	392.3 (88.2)		-5.6
19A325T200-3	200	388.8 (87.4)		-4.8
19A325T400-1	400	310.0 (69.7)	301.2 (67.7)	-2.8
19A325T400-2	400	312.3 (70.2)		-3.5
19A325T400-3	400	314.5 (70.7)		-4.2
19A325T500-1	500	218.0 (49.0)	214.9 (48.3)	-1.4
19A325T500-2	500	232.6 (52.3)		-7.6
19A325T500-3	500	216.6 (48.7)		-0.8
19A325T600-1	600	122.3 (27.5)	126.6 (28.5)	3.5
19A325T600-2	600	134.8 (30.3)		-6.0
19A325T600-3	600	124.1 (27.9)		2.0
|Average|	-	-	-	**3.5**
22A325T20-1	20	540.5 (121.5)	533.1 (119.8)	-1.4
22A325T20-2	20	528.0 (118.7)		1.0
22A325T20-3	20	540.5 (121.5)		-1.4
22A325T20-4	20	523.6 (117.7)		1.8
22A325T200-1	200	503.5 (113.2)	519.5 (116.8)	3.2
22A325T200-2	200	514.2 (115.6)		1.0
22A325T200-3	200	517.8 (116.4)		0.3
22A325T400-1	400	464.4 (104.4)	422.7 (95.0)	-9.0
22A325T400-2	400	443.0 (99.6)		-4.6
22A325T400-3	400	444.4 (99.9)		-4.9
22A325T500-1	500	332.7 (74.8)	301.6 (67.8)	-9.4
22A325T500-2	500	304.3 (68.4)		-0.9
22A325T500-3	500	294.5 (66.2)		2.4
22A325T600-1	600	172.1 (38.7)	177.7 (40.0)	3.2
22A325T600-2	600	182.8 (41.1)		-2.8
22A325T600-3	600	179.3 (40.3)		-0.9
|Average|	-	-	-	**3.0**

Table 4: Summary of measured and predicted double-shear capacities for 19 mm (3/4 in) and 22 mm (7/8 in) diameter A490 high-strength bolts.

Specimen Name	T °C	Meas. Failure Load, kN (kip)	Pred. Failure Load, kN (kip)	Percent Difference
19A490T20-1	20	414.6 (93.2)	419.6 (94.3)	1.2
19A490T20-2	20	415.0 (93.3)		1.1
19A490T20-3	20	429.3 (96.5)		-2.2
19A490T200-1	200	412.4 (92.7)	413.7 (93.0)	0.3
19A490T200-2	200	398.6 (89.6)		3.8
19A490T200-3	200	420.4 (94.5)		-1.6
19A490T400-1	400	347.4 (78.1)	341.7 (76.8)	-1.7
19A490T400-2	400	355.0 (79.8)		-3.7
19A490T400-3	400	364.8 (82.0)		-6.3
19A490T500-1	500	258.4 (58.1)	250.7 (56.4)	-3.0
19A490T500-2	500	262.9 (59.1)		-4.6
19A490T500-3	500	259.3 (58.3)		-3.3
19A490T600-1	600	158.4 (35.6)	162.8 (36.6)	2.8
19A490T600-2	600	163.7 (36.8)		-0.5
19A490T600-3	600	161.0 (36.2)		1.1
|Average|	-	-	-	**2.5**
22A490T20-1	20	568.5 (127.8)	577.2 (129.8)	1.5
22A490T20-2	20	575.2 (129.3)		0.4
22A490T20-3	20	588.1 (132.2)		-1.8
22A490T200-1	200	537.8 (120.9)	569.1 (127.9)	5.8
22A490T200-2	200	549.4 (123.5)		3.6
22A490T200-3	200	555.6 (124.9)		2.4
22A490T400-1	400	480.9 (108.1)	470.0 (105.7)	-2.3
22A490T400-2	400	450.2 (101.2)		4.4
22A490T400-3	400	466.6 (104.9)		0.7
22A490T500-1	500	357.2 (80.3)	344.9 (77.5)	-3.5
22A490T500-2	500	352.7 (79.3)		-2.2
22A490T500-3	500	363.0 (81.6)		-5.0
22A490T600-1	600	206.4 (46.4)	223.9 (50.3)	8.5
22A490T600-2	600	214.8 (48.3)		4.2
22A490T600-3	600	224.2 (50.4)		-0.1
|Average|	-	-	-	**3.1**

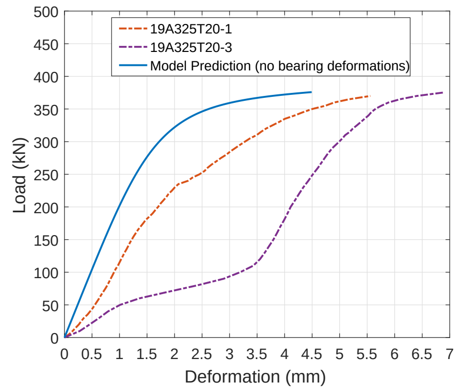

Figure 15: Effect of accumulated bearing deformations on 19 mm (3/4 in) diameter bolt tests.

the predicted double-shear capacity is larger than the experimentally measured double shear capacity, while a positive value for the percent error indicates that the predicted double-shear capacity is smaller than the experimentally measured double shear capacity. The reported averages in Tables 3 and 4 correspond to the average of the absolute value of the percent differences across the full range of test temperatures.

Tables 3 and 4 also show that the percent difference between the predicted bolt double-shear capacity and the measured bolt double-shear capacity tends to increase with increasing temperature, with the predicted capacities at 500 °C and 600 °C on-average having the largest percent differences. This trend could be rationally expected, due to contributions from the combined uncertainties in the deformation at failure and the plastic stiffness in the measured data at these temperatures.

6. Consolidation and Simplification of Component-Based Model

With only a minor loss of accuracy relative to the separately fitted models for the grade A325 and A490 high-strength bolt materials presented in Section 4.2, the component-based model can be consolidated to a single model that is applicable to both types of high-strength bolts. Fig. 16(a) shows a comparison between the retained ultimate tensile strengths for the grade A325 and A490 bolt materials. The retained mechanical properties of the bolt materials are calculated simply as the values of the mechanical properties at elevated temperatures normalized by their mean value at ambient temperature, $\mu_{F_{\mathrm{u,amb}}}$. Both material grades exhibit

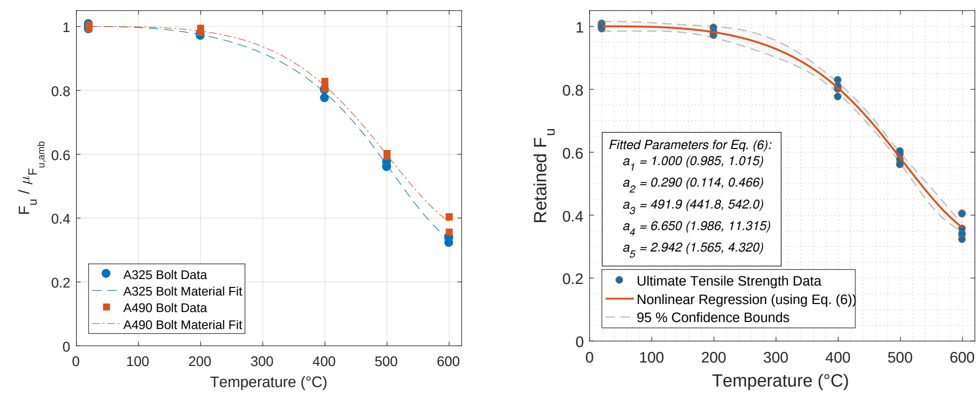

(a) (b)

Figure 16: (a) comparison of individually fitted retained ultimate tensile strength curves for 25 mm (1 in) diameter grade A325 and A490 bolts and (b) aggregated ultimate tensile strength, fitted using Eq. (6).

similar trends, having relatively little degradation at 200 °C after which the rate of degradation increases with increasing temperature. Clearly, the retained ultimate tensile strength of the grade A325 bolt material is less than that of the grade A490 bolt material, indicating that the grade A325 bolt material degraded faster than the grade A490 bolt material with increasing temperature. However, the difference in the retained ultimate tensile strengths of the two bolt materials is relatively minor, differing by only 5.5 % at the maximum considered temperature of 600 °C (the ultimate tensile strength of the grade A325 and A490 bolt materials were on average, 33.3 % and 38.8 %, respectively, of their ambient-temperature ultimate tensile strengths). Fig. 16(b) shows the consolidated fit to the bolt ultimate tensile strength data results, determined by fitting Eq. (6) to the aggregated data for both the grade A325 and A490 bolt materials. The fitted coefficients, a_1 through a_5, along with their 95 % confidence bounds, are shown in the textbox embedded in Fig. 16(b).

A similar consolidation strategy can be considered for the modulus of elasticity data. Fig. 17(a) shows a comparison between the retained modulus of elasticity of the grade A325 and A490 bolt materials. The fitted curves for the modulus of elasticity show that for both bolt materials, the modulus is degraded only slightly at or below 400 °C, but then begins to degrade rapidly at temperatures above 400 °C. At 600 °C, the retained modulus of elasticity of the grade A325 and

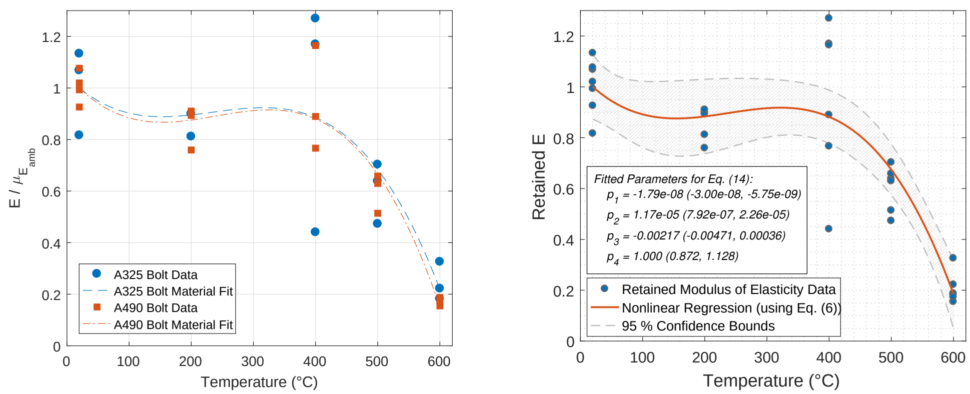

(a) (b)

Figure 17: (a) comparison of individually fitted retained modulus of elasticity curves for 25 mm (1 in) diameter grade A325 and A490 bolts and (b) aggregated modulus of elasticity, fitted using Eq. (14).

A490 bolt materials were on average, 24.3 % and 17.2 %, respectively, of their ambient-temperature values. Despite the obvious scatter in the modulus of elasticity data, particularly for the tests at 400 °C, both the fitted retained modulus of elasticity curves for two bolt materials are barely distinguishable from one another. The close proximity of these two curves indicates that the bolt grade does not significantly influence the modulus of elasticity, even at elevated temperatures. Fig. 17(b) shows the fit of Eq. (14) to the aggregated bolt modulus of elasticity data for both the grade A325 and A490 bolt materials, with the fitted coefficients and their 95 % confidence bounds shown in the textbox.

It was previously noted in Section 4.2 that the shape parameter n had relatively little influence on the calculated capacity of the bolts. The shape parameter likewise has relatively little influence on the initial response of the bolt load-deformation behavior, before appreciable plastic deformations have occurred. To simplify the formulation of the consolidated component-based model, the shape parameter is approximated as a constant value over all temperatures, and is calculated as the average of the consolidated shape parameter data from both the grade A325 and A490 bolts (Fig. 18(a)). A similar strategy is adopted for the ratio of the plastic stiffness to the initial stiffness (Fig. 18(b)). Use of average values for the shape parameter and stiffness ratio reduces the dependence of the component-based model on temperature. The consolidated simplified component-

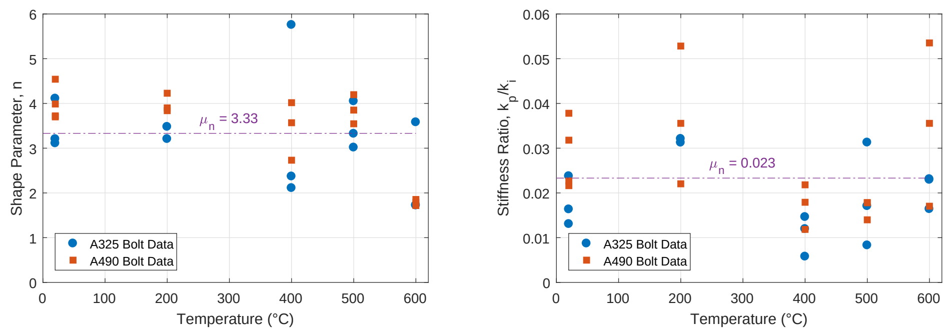

(a) (b)

Figure 18: Aggregated 25 mm (1 in) diameter grade A325 and A490 bolt data for (a) shape parameter, and (b) ratio of plastic stiffness to initial stiffness.

based model depends only the temperature-dependent retained ultimate tensile strength and the temperature-dependent retained modulus of elasticity.

Fig. 19 shows the predicted bolt double-shear load-deformation behavior from the consolidated component-based model, using the fitted curves to the retained ultimate tensile strength (Fig. 16(b)), retained modulus of elasticity (Fig. 17(b)), average shape parameter (Fig. 18(a)), and average stiffness ratio (Fig. 18(b)). Comparison of Fig. 14 and Fig. 19 shows that using the consolidated ultimate tensile strength and modulus of elasticity data, with average values for the shape parameter and stiffness ratio, results in only a slight loss of accuracy with respect to the measured bolt double-shear load-deformation responses. Even when using the simplified component-based model, the predicted response is still typically within the area bounded by the responses of the nominally identical tests. Where the simplified component-based model does predict loads outside the variation between nominal identical tests is typically only at the peak bolt deformation, where the predicted response differs from the nearest experimental response by a maximum of 6.5 % for the grade A325 bolts and 8.4 % for the grade A490 bolts.

7. Assumptions and Limitations

The component-based modeling approach presented in this paper assumed that the deformations in the loading and reaction blocks are sufficiently small to be neglected, and that deformations are concentrated in the bolt in the vicinity of the lapped joints. Since only a small portion of the deformations went into the loading block and reaction blocks (less than 1 % for tests at temperatures up to the

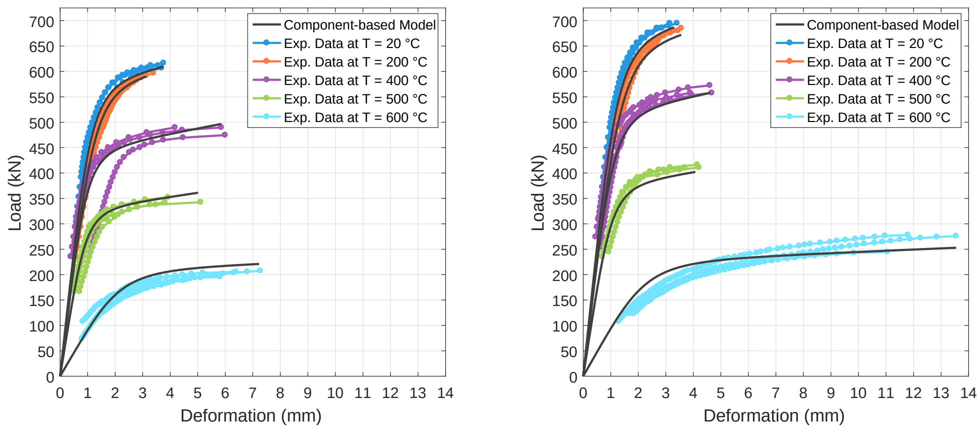

(a)

(b)

Figure 19: Comparison of consolidated, simplified component-based model to experimental data for 25 mm (1 in) diameter (a) A325 bolts and (b) A490 bolts.

600 °C), the approximation of using rigid blocks is reasonable for modeling the 25 mm (1 in) diameter bolt tests reported in Peixoto et al. (2017). However, this assumption would almost certainly not be valid for modeling realistic connection configurations (e.g., steel single-plate shear connections), which have plates that are not heat-treated and thicknesses typically on the order of one-half of the bolt diameter. To accurately model connection behavior at elevated temperatures, the model for temperature-dependent bolt behavior of the bolt presented in this paper can be integrated with additional temperature-dependent plate component springs that capture the temperature-dependent friction-slip and bearing behaviors (Weigand, 2016). The presented modeling approach also implicitly assumes, by using the same deformation capacities for the three bolt diameters, that the deformation capacities of the bolts are relatively insensitive to their diameter, at least within the tested range of diameters between 19 mm (3/4 in) and 25 mm (1 in).

8. Summary and Conclusions

This paper has described the development of a semi-empirical component-based modeling approach for the shear behavior of high-strength bolts at elevated temperatures developed based on the comprehensive set of 25 mm (1 in) bolt double-shear tests from Peixoto et al. (2017). The component-based model separately covers both ASTM A325 and ASTM A490 high-strength bolt materials, and is capable of capturing temperature-induced degradation in both the bolt shear strength and stiffness. A more simplified, consolidated version of the component-based modeling approach was also presented, which predicted the bolt double-shear load deformation response using only the bolt materials' retained ultimate tensile strength and modulus of elasticity. The more simplified model was shown to predict the double-shear load of the bolt within 8.4 % over the full range of tested temperatures from 20 °C to 600 °C.

The degradation in the ultimate tensile strength of the bolt materials with increasing temperature was characterized using the degradation in the bolt double-shear strength. The estimated values for the bolt steel ultimate tensile strength at ambient temperature, based on the bolt double-shear capacities, were shown to be within 6 % and 1 % of the measured ultimate tensile strengths for the A325 and A490 bolts measured using tensile bolt-coupon testing. The other aspects of the bolt double-shear response were characterized by fitting a four-parameter nonlinear equation to the experimental shear load-displacement data for each bolt-test. Results showed that the developed model accurately captures the temperature-induced degradation in bolt shear strength and stiffness of the high-strength bolts at elevated temperatures under shear loading. In comparison to the 25 mm (1 in) diameter bolt data, the accuracy of the model was within the experimental uncertainty between replicate tests.

While the formulation for the bolt load-deformation response was developed based solely on the data from the 25 mm (1 in) diameter bolts, application of the modeling approach to data from the 19 mm (3/4 in) and 22 mm (7/8 in) diameter bolts from Peixoto et al. (2017) demonstrated the model's predictive capabilities. Results showed that the model predicted the double-shear capacities of the 19 mm (3/4 in) and 22 mm (7/8 in) bolts within 10 % for each tested bolt, and within an average percent difference of less than 4 % across the full range of tested temperatures for each combination of bolt diameter and grade. Results also showed that the percent difference between the predicted bolt double-shear capacity and the measured bolt double-shear capacity tended to increase with increasing temperature.

Acknowledgments

The authors would like to thank the National Institute of Standards and Technology (NIST), the Coordination for the Improvement of Higher Education Personnel (CAPES), and the National Council for Scientific and Technological Development (CNPq) for providing testing materials and funding for this research.

The authors would also like to thank the technicians in the Structures Laboratory at UNICAMP, Campinas, Brazil (LabDES), who contributed to the bolt double-shear testing.

Disclaimer

Certain commercial entities, equipment, products, or materials are identified in this document in order to describe the presented modeling procedure adequately. Such identification is not intended to imply recommendation, endorsement, or implication that the entities, products, materials, or equipment are necessarily the best available for the purpose.

References

M. Seif, J. A. Main, T. McAllister, Performance of Steel Shear Tab Connections at Elevated Temperatures, in: Proceedings of the Annual Stability Conference, Structural Stability Research Council, St. Louis, Missouri, 2013.

M. Seif, T. McAllister, J. Main, W. Luecke, Modeling of moment connections for structural fire analyses, AISC Engineering Journal 53 (1) (2016) 47–60.

B. C. Gowda, Tensile properties of SA516, grade 55 steel in the temperature range of 25 °C – 927 °C and strain rate range of 10^{-4} to 10^{-1} sec^{-1}, in: 1978 ASME/CSME Montreal Pressure Vessel & Piping Conference, Montreal, Quebec, Canada, 1978.

W. E. Luecke, J. D. McColskey, C. N. McCowan, S. W. Banovic, R. J. Fields, T. Foecke, T. A. Siewert, F. W. Gayle, Robustness of Steel Gravity Frame Systems with Single-Plate Shear Connections, Tech. Rep. NIST-TN-1749, National Institute of Standards and Technology, United States Department of Commerce, 2005.

G. Hu, M. A. Morovat, J. Lee, E. Schell, M. Engelhardt, Performance of Steel Shear Tab Connections at Elevated Temperatures, in: Proceedings of the ASCE/SEI Structures Congress, Austin, Texas, 1067–1076, 2009.

V. Kodur, S. Kand, W. Khaliq, Effect of Temperature on Thermal and Mechanical Properties of Steel Bolts, Journal of Materials in Civil Engineering 24 (6) (2012) 765–774.

L. Yu, Behavior of Bolted Connections During and After a Fire, Ph.D. Dissertation in the Department of Civil, Architectural and Environmental Engineering, The University of Texas at Austin, Austin, TX, 2006.

E. C. Fischer, A. H. Varma, Q. Zhu, Behavior of Single-Bolted Lap-Splice Joints at Elevated Temperatures, in: Proceedings of the Eighth International Workshop on Connections in Steel Structures (Connections VIII), Boston, MA, 2016.

R. M. Peixoto, M. S. Seif, L. C. Viera, Double-shear tests of high-strength structural bolts at elevated temperatures, Fire Safety Journal .

ASTM, Standard Specification for Structural Bolts, Heat Treated 830 MPa Minimum Tensile Strength (Metric), American Society for Testing and Materials (ASTM) International, West Conshohocken, PA, 2014a.

ASTM, Standard Specification for High-Strength Steel Bolts, Classes 10.9 and 10.3, for Structural Steel Joints (Metric), American Society for Testing and Materials (ASTM) International, West Conshohocken, PA, 2014b.

ASTM, Standard Specification for Carbon Structural Steel, American Society for Testing and Materials (ASTM) International, West Conshohocken, PA, 2014c.

J. M. Weigand, Component-Based Model for Single-Plate Shear Connections with Pretension and Pinched Hysteresis, Journal of Structural Engineering (2016) 04016178.

J. M. Weigand, The Integrity of Steel Gravity Framing System Connections Subjected to Column Removal Loading, Ph.D. Dissertation in Civil Engineering, University of Washington, Seattle, WA, 2014.

J. Crocker, J. Chambers, Single plate shear connection response to rotation demands imposed by frames undergoing cyclic lateral displacements, Journal of Structural Engineering 130 (6) (2004) 934–941.

J. M. Weigand, J. W. Berman, Integrity of Steel Single Plate Shear Connections Subjected to Simulated Column Removal, Journal of Structural Engineering 140 (5) (2014) 04013114.

R. M. Richard, B. J. Abbott, Versatile Elastic-Plastic Stress-Strain Formulation, Journal of the Engineering Mechanics 101 (EM4) (1975) 511–515.

Z. Ugray, L. Lasdon, J. Plummer, F. Glover, J. Kelly, R. Marti, Scatter Search and Local NLP Solvers: A Multistart Framework for Global Optimization, INFORMS Journal on Computing 19 (3) (2007) 328–340.

MathWorks, MATLAB Global Optimization Toolbox User's Guide, Version 3.4.1 (R2016b), The MathWorks, Inc., Natick, Massachusetts, United States, 2016.

W. D. Nelson, B. L. Bunin, L. J. Hart-Smith, Critical Joints in Large Composite Aircraft Structure, Tech. Rep. NASA Contractor Report 3710, Douglas Aircraft Company, McDonnell Douglas Corporation, 1983.

D. L. Thomas, J. M. Wilson, R. R. Wilson, Timoshenko Beam Finite Elements, Journal of Sound and Vibration 31 (3) (1973) 315–330.

S. H. Hsieh, G. G. Deierlein, Nonlinear Analysis of Three-Dimensional Steel Frames with Semi-Rigid Connections, Computers & Structures 41 (5) (1990) 995–1009.

Appendix A. Generalization of Bolt Shear Load Deformation Response for Cyclic Behavior

Although the bolt double-shear load-deformation response considered in this paper was uniaxial, the empiracle model for the bolt shear load-deformation behavior can be readily generalized to consider cyclic behavior, using the modification to the Richard Equation proposed by Hsieh and Deierlein (1990):

$$P(\delta) = P_{\mathrm{unl}} + \frac{\left(k_{\mathrm{i}} - k_{\mathrm{p}}\right)(\delta - \delta_{\mathrm{unl}})}{\left(1 + \left|\frac{\left(k_{\mathrm{i}} - k_{\mathrm{p}}\right)(\delta - \delta_{\mathrm{unl}})}{r_{\mathrm{n,cyc}}}\right|^{n}\right)^{(1/n)}} + k_{\mathrm{p}}(\delta - \delta_{\mathrm{unl}}) \quad , \tag{A.1}$$

where δ, k_{i} and k_{p}, n, are as defined for Eq. (1). In the cyclic form in Eq. (A.1), the reference load R_{n} becomes a cyclic reference load $r_{\mathrm{n,cyc}}$ with $r_{\mathrm{n,cyc}} = r_{\mathrm{n}}$ for the first cycle and $r_{\mathrm{n,cyc}} = \mathrm{sign}(\delta - \delta_{\mathrm{unl}})r_{\mathrm{n}} - r_{\mathrm{unl}} + k_{\mathrm{p}}\delta_{\mathrm{unl}}$ for subsequent cycles, and $(\delta_{\mathrm{unl}}, R_{\mathrm{unl}})$ are the coordinates of the previous unload point ($\delta_{\mathrm{unl}} = 0$ and $R_{\mathrm{unl}} = 0$ for the first cycle). Eq. (A.1) results in full cyclic hysteresis loops with no pinching and kinematic hardening (i.e., translation of hysteresis loops at increasing center displacements along a line through the origin with a slope of the plastic stiffness).

The cyclic form of the Richard Equation, including temperature-dependence, is thus

$$P(\delta, T) = P_{\mathrm{unl}} + \frac{\left(k_{\mathrm{i}}(T) - k_{\mathrm{p}}(T)\right)(\delta - \delta_{\mathrm{unl}})}{\left(1 + \left|\frac{\left(k_{\mathrm{i}}(T) - k_{\mathrm{p}}(T)\right)(\delta - \delta_{\mathrm{unl}})}{r_{\mathrm{n,cyc}}(T)}\right|^{n(T)}\right)^{\left(1/n(T)\right)}} + k_{\mathrm{p}}(T)(\delta - \delta_{\mathrm{unl}}) \quad , \qquad \text{(A.2)}$$

where (T) denotes dependence on temperature, $r_{\mathrm{n,cyc}} = r_{\mathrm{n}}(T)$ (for the first cycle) and $r_{\mathrm{n,cyc}}(T) = \mathrm{sign}(\delta - \delta_{\mathrm{unl}}) r_{\mathrm{n}}(T) - r_{\mathrm{unl}} + k_{\mathrm{p}}(T)\delta_{\mathrm{unl}}$ (for subsequent cycles), with the parameters $k_{\mathrm{i}}(T)$, $k_{\mathrm{p}}(T)$, $r_{\mathrm{n}}(T)$, and $n(T)$ determined using Eq. (5) through (14).